Structural studies of viperin, an antiviral radical SAM enzyme

Michael K. Fenwick[a,1], Yue Li[b,1], Peter Cresswell[b,2], Yorgo Modis[c,2], and Steven E. Ealick[a,2]

[a]Department of Chemistry and Chemical Biology, Cornell University, Ithaca, NY 14853; [b]Department of Immunobiology, Yale University School of Medicine, New Haven, CT 06520; and [c]Department of Medicine, University of Cambridge, Medical Research Council Laboratory of Molecular Biology, Cambridge CB2 0QH, United Kingdom

Contributed by Peter Cresswell, May 16, 2017 (sent for review March 31, 2017; reviewed by Steven C. Almo, Juan C. Fontecilla-Camps, and Hazel Holden)

Viperin is an IFN-inducible radical *S*-adenosylmethionine (SAM) enzyme that inhibits viral replication. We determined crystal structures of an anaerobically prepared fragment of mouse viperin (residues 45–362) complexed with *S*-adenosylhomocysteine (SAH) or 5′-deoxyadenosine (5′-dAdo) and L-methionine (L-Met). Viperin contains a partial $(\beta\alpha)_6$-barrel fold with a disordered N-terminal extension (residues 45–74) and a partially ordered C-terminal extension (residues 285–362) that bridges the partial barrel to form an overall closed barrel structure. Cys84, Cys88, and Cys91 located after the first β-strand bind a [4Fe-4S] cluster. The active site architecture of viperin with bound SAH (a SAM analog) or 5′-dAdo and L-Met (SAM cleavage products) is consistent with the canonical mechanism of 5′-deoxyadenosyl radical generation. The viperin structure, together with sequence alignments, suggests that vertebrate viperins are highly conserved and that fungi contain a viperin-like ortholog. Many bacteria and archaebacteria also express viperin-like enzymes with conserved active site residues. Structural alignments show that viperin is similar to several other radical SAM enzymes, including the molybdenum cofactor biosynthetic enzyme MoaA and the RNA methyltransferase RlmN, which methylates specific nucleotides in rRNA and tRNA. The viperin putative active site contains several conserved positively charged residues, and a portion of the active site shows structural similarity to the GTP-binding site of MoaA, suggesting that the viperin substrate may be a nucleoside triphosphate of some type.

radical SAM | IFN-stimulated gene | antiviral cellular factor | free radical | *S*-adenosyl methionine

Viruses exploit the metabolic machinery of host cells to replicate and spread to other cells. Although cytotoxic T cells and antibody-producing B cells can ultimately be produced in an adaptive response to the virus, innate immune mechanisms are used to respond to infection rapidly. Upon infection, cells can sense the presence of virus via pattern recognition receptors (1, 2) and produce IFNs that limit the spread of infection to other cells (3). IFNs induce the expression of hundreds of IFN-stimulated genes (ISGs), many of which are involved in various antiviral processes, including antigen presentation, apoptosis, and inhibition of viral replication (4–7).

Viperin, the product of *rsad-2*, was first identified as a protein induced by exposure of human macrophages to IFN-γ and by infection of primary human fibroblasts with human cytomegalovirus (8, 9). Early studies showed that viperin is induced in various cell types by IFN-α and IFN-β, associates with the cytosolic face of the endoplasmic reticulum (ER), and inhibits human cytomegalovirus replication when preexpressed in human fibroblasts (8). Since then, viperin has been shown to be induced by several factors, including lipopolysaccharide (10–12), and to inhibit a broad range of viruses, including HIV-1 (13), West Nile virus (14), hepatitis C virus (15, 16), dengue virus type 2 (17), influenza A virus (18), and tick-borne encephalitis virus (19). Gene-profiling microarray studies have shown that the viperin gene is one of the most highly inducible ISGs upon infection with a wide range of RNA viruses (20).

The amino acid sequence of viperin contains a CxxxCxxC motif, characteristic of the radical *S*-adenosylmethionine (SAM) superfamily (8, 21), which is usually characterized structurally by a $(\beta\alpha)_8$-barrel or partial $(\beta\alpha)_6$-barrel fold (22). Radical SAM enzymes use a [4Fe-4S] cluster to cleave SAM reductively to generate a radical, which is typically transferred to a substrate via hydrogen atom abstraction (23–31). The cysteine residues within the CxxxCxxC motif ligate three of the iron atoms of the [4Fe-4S] cluster. Recombinant viperin has been shown to bind a [4Fe-4S] cluster and reductively cleave SAM (32), and mutation of the cysteine residues of the CxxxCxxC motif to alanine significantly diminishes the antiviral effects of viperin in HIV-1–infected cells (13) or hepatitis C virus-infected cells (16). Although viperin appears to be a radical SAM enzyme, neither the reaction it catalyzes nor its substrate has been identified.

In the present study, we prepared and crystallized *Mus musculus* viperin under anaerobic conditions and determined crystal structures of viperin complexes with the SAM analog *S*-adenosylhomocysteine (SAH) or the SAM cleavage products 5′-deoxyadenosine (5′-dAdo) and L-methionine (L-Met). The structures reveal the active site architecture and identify key active site residues. The active site architecture, together with multiple sequence alignments, shows that vertebrate viperins are highly conserved and that fungi, bacteria, and archaebacteria express viperin-like enzymes. Structural alignments show similarity between viperin and the molybdenum cofactor biosynthetic enzyme MoaA and the RNA methyltransferase RlmN. The similarity extends to portions of the viperin and MoaA active sites.

Significance

We report structures of viperin, an antiviral radical *S*-adenosylmethionine (SAM) enzyme. The overall structure shows a canonical radical SAM enzyme fold that harbors a [4Fe-4S] cluster. Structures with a bound SAM analog or SAM cleavage products are consistent with a conventional mechanism of radical formation. Sequence alignments guided by the putative active site residues of viperin reveal viperin-like enzymes in species from all kingdoms of life. Structural alignments show similarity between viperin and the molybdenum cofactor biosynthetic enzyme MoaA and show that the active site architecture of viperin is consistent with a nucleoside triphosphate substrate.

Author contributions: M.K.F., Y.L., P.C., Y.M., and S.E.E. designed research; M.K.F., Y.L., and Y.M. performed research; M.K.F., Y.L., Y.M., and S.E.E. analyzed data; and M.K.F., Y.L., P.C., Y.M., and S.E.E. wrote the paper.

Reviewers: S.C.A., Albert Einstein College of Medicine; J.C.F.-C., Institut de Biologie Structurale; and H.H., University of Wisconsin.

The authors declare no conflict of interest.

Data deposition: The coordinates of viperin with bound *S*-adenosylhomocysteine and with bound 5′-deoxyadenosine and L-methionine have been deposited in the Protein Data Bank, www.pdb.org (PDB ID codes 5VSL and 5VSM).

[1]M.K.F. and Y.L. contributed equally to this work.

[2]To whom correspondence may be addressed. Email: peter.cresswell@yale.edu, ymodis@mrc-lmb.cam.ac.uk, or see3@cornell.edu.

This article contains supporting information online at www.pnas.org/lookup/suppl/doi:10.1073/pnas.1705402114/-/DCSupplemental.

Results and Discussion

Crystallization and Structure Determination. We crystallized an N-terminally truncated (Δ44 or Δ46) form of *M. musculus* viperin containing a [4Fe-4S] cluster under anaerobic conditions. The truncation removes an amphipathic α-helix near the N terminus responsible for ER and lipid droplet association and results in a water-soluble derivative (33, 34). Crystal structures were determined for viperin bound to SAH at 2.0 Å resolution and to 5′-dAdo and L-Met at 1.7 Å resolution (Tables S1 and S2). The crystals belong to space group $P2_12_12_1$, and the asymmetric unit contains two molecules of viperin, each with ligands bound. Electron density maps show clear electron density for the ligands and high occupancies for the four iron atoms of the [4Fe-4S] cluster (Fig. S1).

Overall Structure. Viperin is a globular protein containing a partial $(\beta\alpha)_6$-barrel fold (residues 75–284) observed in other radical SAM enzymes (22). Residues 45–73 at the N terminus and residues 337–362 at the C terminus are disordered. The overall fold of viperin is illustrated in Fig. 1 *A* and *B*. The partial $(\beta\alpha)_6$-barrel is augmented by a β-strand (β_7), a β-hairpin (β_8 and β_9), and three α-helices (α_7, α_8, and α_9) from the C-terminal extension. β_7 forms hydrogen bonds with β_6, β_8 forms hydrogen bonds with β_1, and β_7 and β_8 are connected by a segment containing a short α-helix (α_7). The C-terminal extension folds over the open portion of the partial $(\beta\alpha)_6$-barrel, resulting in an overall closed barrel structure similar to a $(\beta\alpha)_8$-barrel. β_9 and α_8 are connected by a 12-residue loop in which $G_{316}GRKD_{320}$ of the loop is disordered. The final 26 residues of the protein, which follow α_9, are disordered. C-terminal truncations have been shown to reduce the effectiveness of viperin against HIV-1 (13), hepatitis C virus (16), and dengue virus type 2 (17), suggesting that the C terminus may be required for interactions with a binding partner. Indeed, viperin interaction with the cytosolic Fe/S cluster assembly factor CIAO1 depends on the conserved viperin C-terminal tryptophan residue, suggesting that viperin lacking the C-terminal region is likely to be enzymatically inactive (19). Residues 50–74 of the N-terminal extension are predicted to be disordered based on analysis of the amino acid sequence (35) (Fig. S2). This region

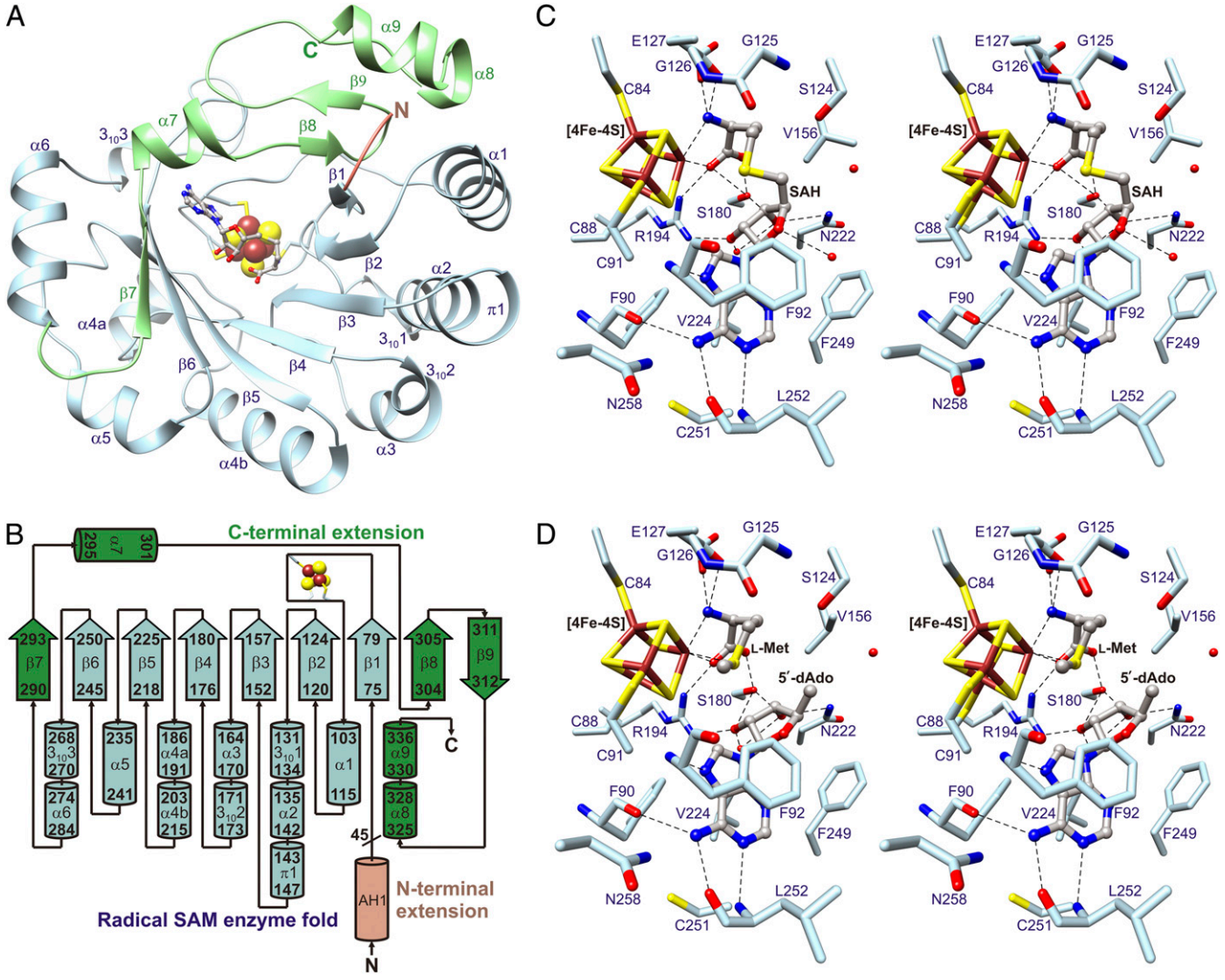

Fig. 1. Overall structure of viperin. (*A*) Ribbon diagram of viperin with SAH shown as balls and sticks, the [4Fe-4S] cluster shown as brown and yellow spheres, and the three cysteine residues of the [4Fe-4S] cluster-binding motif shown as sticks. The partial $(\beta\alpha)_6$-barrel fold, N-terminal extension, and C-terminal extension are colored light blue, salmon, and light green, respectively. (*B*) Topology diagram for viperin. The β-strands and helices are represented by thick arrows and cylinders, respectively. AH1 denotes the excised putative membrane-associating amphipathic helix. (*C*) Stereoview of the SAH-binding site. (*D*) Stereoview of the 5′-dAdo and L-Met binding sites. Potential hydrogen bonds are shown as dashed lines, and water molecules are shown as red spheres.

may act as a flexible linker that aids membrane localization (33, 34) and enhances molecular mobility after localization.

Canonical Radical SAM Enzyme Structure. The viperin β-barrel fold contains the radical SAM enzyme hallmark CxxxCxxC motif (C_{84}NYKC_{88}GFC_{91}) located after strand β_1. The three cysteine side chains of the motif ligate three irons of a [4Fe-4S] cluster and position the differentiated iron (not ligated by a cysteine side chain) near the center of the putative active site. The interactions made between viperin and SAH, 5′-dAdo, and L-Met are consistent with known radical SAM enzyme structures (Fig. 1 *C* and *D*). SAH and L-Met anchor to the differentiated iron of the [4Fe-4S] cluster via their α-amino and α-carboxylate groups (28, 36). The α-amino group also forms hydrogen bonds with a conserved GGE motif ($G_{125}G_{126}E_{127}$) (21, 22), and the α-carboxylate group also forms hydrogen bonds with an arginine and serine side chain (Arg194 and Ser180) (37). The ribose moiety of SAH and 5′-dAdo forms hydrogen bonds with the Arg194 and Ser180 side chains, and its O3′-hydroxyl group is within hydrogen-bonding distance of the side chain of Asn222. The adenine moiety of SAH and 5′-dAdo is interposed between hydrophobic residues in or near the cluster-binding loop (Phe90 and Phe92), in β_5 (Val224), and near the end of β_6 (Phe249 and Leu252). The adenine moiety also forms hydrogen bonds with polar sites near the cluster-binding loop and near the end of β_6 (Fig. 1 *C* and *D*).

The binding modes of SAH and L-Met with the [4Fe-4S] cluster are consistent with the ability of viperin to cleave the C5′-S bond of SAM reductively (32) (Fig. S3) and are similar to the binding modes observed in high-resolution crystal structures of other radical SAM enzymes (28, 38–43) (Fig. S4). In the proposed mechanism of radical generation, a reduced [4Fe-4S] cluster delivers an electron to the sulfonium ion of SAM to cleave the C5′-S bond homolytically (44). This reaction requires a nearly linear arrangement of C5′, S, and Fe (45); typical Fe-S distances are 3.2–3.7 Å, and C5′-S-Fe angles are ∼150° (Fig. 1*C* and Figs. S3*A* and S4*A*). After cleavage of the C5′-S bond, the sulfur atom of L-Met is expected to coordinate to the differentiated iron of the cluster, along with the α-amino and α-carboxylate groups, to form an octahedral coordination sphere (44) (Fig. 1*D* and Figs. S3*B* and S4*B*).

Putative Viperin Active Site. Two narrow passageways lead to the [4Fe-4S] cluster bound to viperin. One has a diameter of 6 Å and forms part of the putative active site cavity, because it leads directly to C5′ of SAH and 5′-dAdo, the site of radical formation (Fig. 2*A*). The second passageway is located on the opposite side of the protein and is formed by Leu264, Arg265, and the cluster-binding loop (Fig. S5). The active site cavity is formed by residues from strands β_1–β_6 and the beginning of the C-terminal extension. These residues line the β-barrel, with their side chains directed toward its interior (Fig. 2*B*). The active site residues supply five positively charged (Lys120, Lys220, Arg245, Lys247, and Lys297), one negatively charged (Glu293), 10 additional hydrophilic, and seven hydrophobic side chains (Fig. 2*B*).

Viperin Crystal Packing Interactions. The asymmetric unit of viperin crystals contains two molecules that interact through several salt bridges that are formed between the positively charged active site residues of one molecule and negatively charged residues in the loop following β_6 of a second molecule (Fig. S6). This head-to-tail interaction, together with the crystallographic twofold screw axis, generates pseudo-fourfold screw axis symmetry along the *c* axis of the unit cell. The interface between the two viperin molecules in the asymmetric unit is relatively small (∼1,000 Å^2) (46), lacks twofold symmetry, and hence is not predicted to result in a dimer in solution. However, it is possible that the head-to-tail interactions observed in the crystal contribute to higher order structures or polymerization when viperin is localized at the ER membrane at high concentrations (34).

Sequence Alignments with *M. musculus* Viperin. Viperin is highly conserved within vertebrates, although significant sequence variation occurs in the N-terminal region that precedes the β-barrel (8, 47). BLAST searches starting with *M. musculus* viperin show that viperin is highly conserved among 171 vertebrates, with sequence identities ranging from roughly 65 to 95%. In addition, the proposed active site residues are conserved. BLAST searches also show a group of closely related fungal enzymes. Sequence alignments show that both the predicted structures and the putative active sites of the fungal viperin-like proteins are conserved compared with viperin. The fungal enzymes lack the N-terminal extension found in viperin but have a C-terminal extension that shows conservation within the fungal enzymes but is distinct from the viperin C-terminal extension, which itself is highly conserved. Although the biological role of the fungal viperin-like enzymes is unknown, it can be safely concluded that viperin and the fungal viperin-like enzymes have the same substrates and/or catalyze the same radical SAM chemistry. BLAST searches also yield many bacterial and archaebacterial enzymes with low sequence identity (20–40%). With the exception of MoaA,

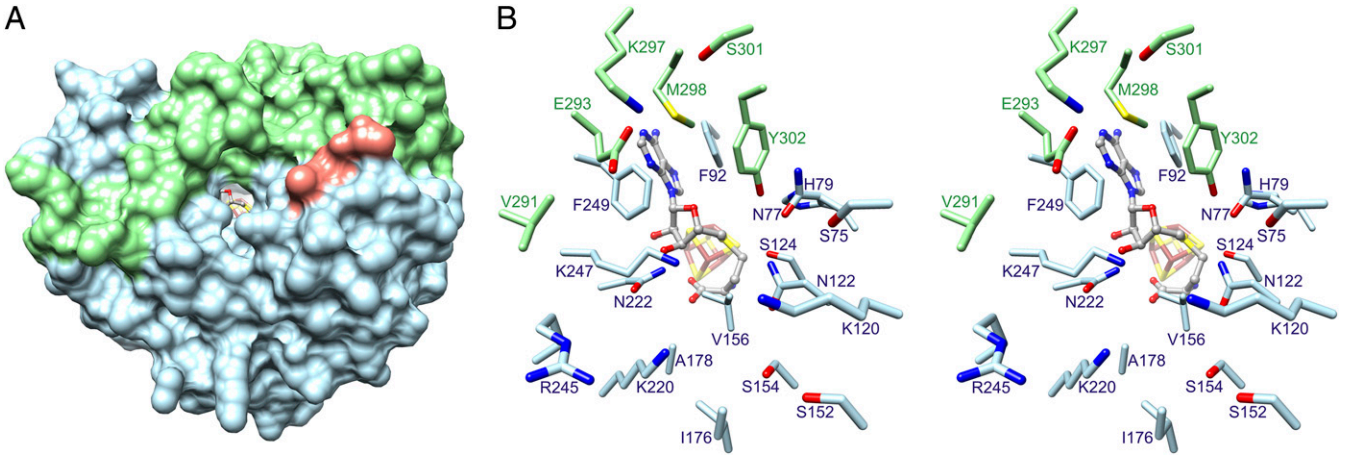

Fig. 2. Structure of the viperin active site cavity. (*A*) Surface representation of viperin showing a narrow passageway leading to C5′ of SAH, the predicted site of radical formation. (*B*) Stereoview of the active site cavity. Residues in the partial $(\beta\alpha)_6$-barrel fold, N-terminal extension, and C-terminal extension are colored light blue, salmon, and light green, respectively.

which is found in both prokaryotes and eukaryotes, these enzymes are best characterized as radical SAM enzymes of unknown function.

Comparison of Viperin and MoaA Structures. A Dali search beginning with viperin shows structural similarity to many radical SAM enzymes (Z-scores ranging from 11 to 20) (48). The most similar structures are the anaerobic sulfatase-maturating enzyme anSME from *Clostridium perfringens* (Z-score of 19.9) (41), MoaA from *Staphylococcus aureus* (49) (Z-score of 18.7), the pyruvate formate-lyase activating enzyme PflA from *Escherichia coli* (Z-score of 18.1) (50), and the dual-specificity RlmN from *E. coli* (Z-score of 17.8) (38, 51). Local sequence alignments of viperin to sequences in the Protein Data Bank (PDB) using BLAST show that *S. aureus* MoaA is the only protein that gives an Expect (E) value less than 10 ($E = 4 \times 10^{-6}$) (52). Furthermore, more than half of ~7,500 sequences (having E values <10) produced from alignments of viperin to the nonredundant protein sequence database using BLAST are predicted to be MoaA.

The results described above led us to examine the similarity between viperin and MoaA (PDB ID code 2FB3) in greater detail. MoaA is widely distributed in both prokaryotes and eukaryotes, where it uses radical chemistry to catalyze the cyclization of GTP to 3′,8-cyclic-GTP in the first step of molybdenum cofactor biosynthesis (53, 54). Superposition of viperin and MoaA shows similar partial $(\beta\alpha)_6$-barrel cores (Fig. 3*A*). In addition, MoaA has a short N-terminal extension, and, like viperin, its C-terminal extension folds over the partial β-barrel and forms a β-hairpin, a loop, and a helical region (49). However, the C-terminal extension of MoaA ligates a second [4Fe-4S] substrate-binding cluster that is not found in viperin. GTP binds to the additional [4Fe-4S] cluster through N1 and the two-amino group of the guanine base.

The superposition of viperin and MoaA results in clashes between the ribose and guanine moieties of GTP and the C-terminal extension of viperin; however, the structures align remarkably well near the triphosphate-binding site of GTP (Fig. 3*B*). Similar modified β-barrels are used by both enzymes to form active site channels lined with several positively charged and other hydrophilic residues (Fig. S7). These residues include Arg17, Lys69, Arg71, Thr102, Asn124, Lys163, Asn165, and Arg192 in MoaA and Lys120, Lys220, Lys247, Arg245, Ser75, Asn77, Asn122, Ser154, and Asn222 in viperin. Moreover, the second β-strand and the following SAM-binding motif of MoaA (K_{69}IRITGGEPL) are very similar to the second β-strand and the following SAM-binding motif of viperin (K_{120}INFSGGEPF), and six active site residues in MoaA (Lys69, Lys163, Arg192, Thr73, Asn165, and Ile194) are similar or identical to and occupy the same locations as six active site residues in viperin (Lys120, Lys220, Lys247, Ser124, Asn222, and Phe249, respectively). The structural comparison shows that viperin likely contains a triphosphate-binding site, and although viperin and MoaA almost certainly catalyze different chemical reactions, the viperin substrate is probably some form of nucleoside triphosphate.

Comparison of Viperin and RlmN Structures. Viperin was recently shown to coprecipitate with dengue virus type 2 RNA (17). RlmN is a radical SAM enzyme that methylates adenosine 2503 of 23S rRNA and adenosine 37 of a subset of tRNAs, and it is the only radical SAM RNA-modifying enzyme for which a structure has been reported (38, 51, 55–57) (Fig. S8*A*). RlmN contains a partial $(\beta\alpha)_6$-barrel core, which superimposes well with the partial $(\beta\alpha)_6$-barrel core of viperin (Dali Z-score of 17.6, Dali rmsd of 2.6 Å), and an N-terminal domain for RNA recognition (Fig. S8*B*). Nucleotides 36–39 of tRNA insert into the active site of RlmN to position A37 for methylation. RlmN binds the 5′-phosphate groups of nucleotides 37–39 via Arg114, Thr116, Asn172, Arg207, Asn307, and Arg344. These residues are similar in type to the residues that bind the triphosphate moiety of GTP in MoaA; however, the architecture is significantly different. Superposition of RlmN/tRNA onto viperin shows numerous clashes between viperin active site side chains and the tRNA loop (Fig. S9). Although phosphate-binding sites are typically formed by positively charged and hydrogen bond-donating residues (58), the local active site architecture surrounding the phosphate groups of a nucleoside triphosphate or RNA would, in general, be expected to be different. Thus, our structural comparisons with MoaA and RlmN, although limited, suggest that the active site of viperin better reflects a binding site for a free or chain-terminal nucleotide than an inner nucleotide of RNA.

Comparison of Predicted Radical SAM Enzymes of Unknown Function with Viperin. Interestingly, a large group of bacterial and archaebacterial radical SAM enzymes of unknown function identified

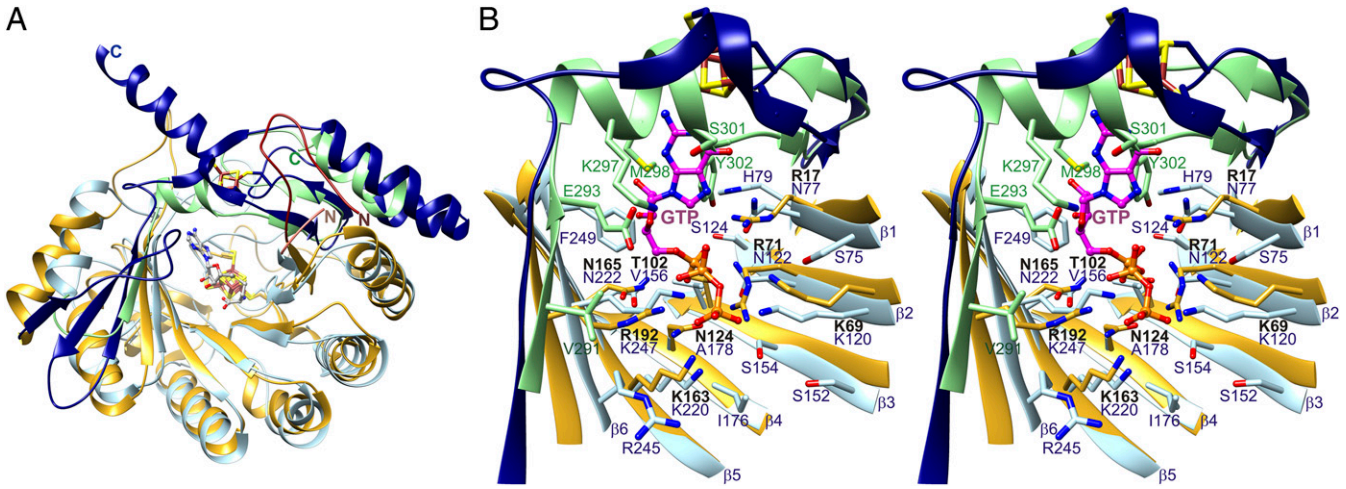

Fig. 3. Structural comparison of viperin and *S. aureus* MoaA. (*A*) Superimposition of MoaA onto viperin. The partial $(\beta\alpha)_6$-barrel fold, N-terminal extension, and C-terminal extension of viperin are colored light blue, salmon, and light green, respectively. The corresponding regions of MoaA are colored goldenrod, dark red, and navy blue. SAH bound to viperin is shown as balls and sticks. GTP bound to MoaA is not shown for clarity. The [4Fe-4S] clusters and the cysteine residues that ligate the irons are shown as sticks. (*B*) Active site comparison of viperin and MoaA. GTP bound to MoaA is shown as balls and sticks. The side chains of 22 active site residues of viperin and the side chains of eight residues of MoaA that reside within 4 Å of the phosphate groups of GTP are shown.

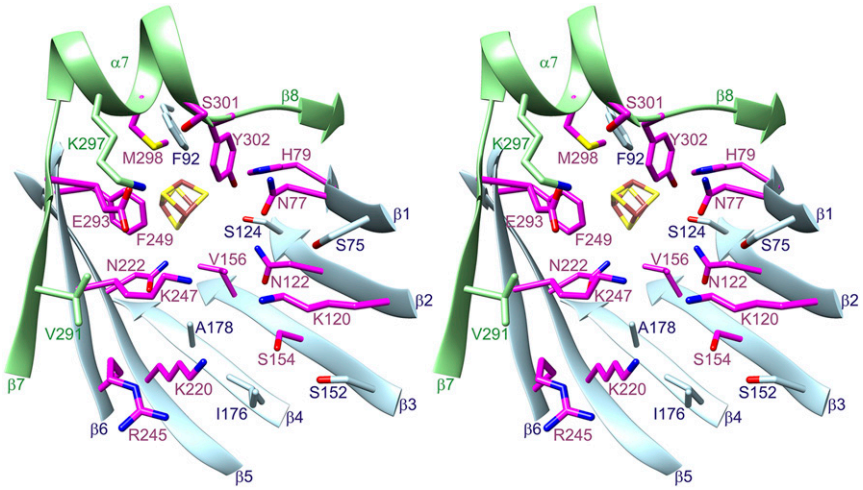

Fig. 4. Stereoview of the viperin active site showing conserved residues found in viperin or viperin-like enzymes from all kingdoms of life. Viperin-like enzymes were identified by searching for the active site residues of *M. musculus* viperin in a large set of sequences aligned to *M. musculus* viperin using BLAST with an E value of 10. Fifteen active site residues (represented with magenta sticks) were found to be conserved.

from BLAST searches show significant similarity to viperin. In general, these viperin-like enzymes lack both the N-terminal extension of viperin and the final 15 C-terminal residues, which are conserved in vertebrate viperins. They also lack the second substrate-binding iron-sulfur cluster found in MoaA, and the sequences are, in general, more similar to viperin than MoaA. Within the active site, 15 mostly charged and hydrophilic residues are conserved compared with viperin (Fig. 4). Sequence alignments further show that these 15 residues are also highly conserved in viperin or viperin-like enzymes found in protists, fungi, and invertebrate and vertebrate animals. In addition, 14 of these residues are conserved in the green alga *Chlamydomonas reinhardtii*. A sequence alignment of viperin with representative enzymes from all kingdoms of life is shown in Fig. S10. The conservation of the active site residues suggests that viperin and this widely distributed group of viperin-like enzymes have the same or similar substrates and/or catalyze the same or similar chemical reactions.

Materials and Methods

Anaerobic Production and Crystallization. Residues 45–362 of *M. musculus* viperin (viperinΔ44) were overexpressed and purified using a variation of the methods used for preparation of radical SAM enzymes involved in thiamin and B_{12} biosynthesis (26, 59). A gene for viperinΔ44 with a cleavable N-terminal hexahistidine tag was synthesized with codon optimization for expression in *E. coli* and cloned into pET-28 via NcoI and XhoI restriction sites to give the following protein product: NH_2-MGSDKIHHHHHHSSGENLYFQG$_{45}$...W_{362}-COOH. A second truncated form of viperin lacking the first 46 amino acids, viperinΔ46, was prepared without gene optimization, and was overexpressed and purified using similar procedures: MGSSHHHHHHSSGRENLYFQGHMASMTGGQQMGRGSE$_{47}$...W_{362}-COOH. *E. coli* NiCo21(DE3) cells (New England Biolabs) that contained plasmid pSuf (60) were transformed with the plasmid carrying the recombinant viperin gene. Starter cultures grown in 15 mL of lysogeny broth supplemented with kanamycin (40 mg/L) and chloramphenicol (34 mg/L) were transferred to shaker flasks containing 1.85 L of minimal medium (1× minimal medium salts, 40 mg/L kanamycin, 34 mg/L chloramphenicol, 4 g/L dextrose, 2 mM $MgSO_4$, and 0.1 mM $CaCl_2$). The cultures were shaken at 180 rpm and 37 °C until the OD_{600} reached 0.5–0.55, and were then placed in a 4 °C cold room for 2.5 h. L-Cys, $Fe(NH_4)_2(SO_4)_2$, and isopropyl β-D-1-thiogalactopyranoside were added to final concentrations of 0.21 mM, 0.065 mM, and 0.2 mM, respectively, and the cultures were shaken at 50 rpm and 15 °C for 20 h. The cultures were then chilled to 4 °C, and the *E. coli* cells were harvested via centrifugation at 6,000 × *g* and 4 °C for 15 min and then flash-frozen in liquid nitrogen.

Frozen cell pellets were thawed in a PVC anaerobic chamber (Coy Laboratory Products), resuspended in lysis buffer [100 mM Tris·HCl, 5 mM dithiothreitol (DTT), 0.4 mg/mL lysozyme, and 1.9 kU benzonase (pH 7.6)], incubated for 30–60 min on ice, and lysed further via sonication. The lysate was sealed in centrifuge bottles, transferred to a centrifuge outside of the glove box, and spun at 60,000 × *g* and 4 °C for 20 min. The spun lysate was brought back into the glove box, and the supernatant was subjected to immobilized nickel affinity chromatography using wash [50 mM Tris·HCl, 300 mM NaCl, 20 mM imidazole, and 3 mM DTT (pH 7.4)] and elution [50 mM Tris·HCl, 300 mM NaCl, 250 mM imidazole, and 3 mM DTT (pH 7.5)] buffers. The eluate was buffer-exchanged into hexahistidine tag cleavage buffer [25 mM Tris·HCl, 125 mM NaCl, and 3 mM DTT (pH 7.5)] using a Bio-Rad Econo-Pac 10DG desalting column and incubated for 8 h with tobacco etch virus protease. The reaction mixture was subjected to subtractive immobilized nickel affinity chromatography, buffer-exchanged into 5 mM Hepes and 25 mM NaCl (pH 7.1), and flash-frozen in liquid nitrogen.

ViperinΔ44 and viperinΔ46 with bound SAH and viperinΔ44 with bound 5′-dAdo and L-Met were crystallized inside the anaerobic chamber at room temperature using the hanging drop vapor diffusion method. Drops were prepared with a 1:1 ratio of protein-to-reservoir solution. The concentration of viperin was ∼0.2 mM, and the concentrations of SAH (solubilized in dimethyl sulfoxide), 5′-dAdo, and L-Met were 5 mM, 5 mM, and 10 mM, respectively. Typical reservoir solutions contained 100 mM Hepes (pH 7.0–7.6) and 10–30% (wt/vol) polyethylene glycol monomethyl ether (PEG MME) 2,000; the concentration of PEG MME 2,000 was increased 5–25% in the cryoprotectant.

X-Ray Data Collection and Processing. Viperin crystals were exposed to X-rays with wavelengths λ = 0.9792 Å, λ = 0.9793 Å, or λ = 1.7384 Å at 100 K at beamline NE-CAT 24-ID-C of the Advanced Photon Source (Table S1). X-ray diffraction images were recorded at oscillations of 1° per second on a PILATUS 6MF detector positioned 290 mm (λ = 0.9792 Å), 390 mm (λ = 0.9793 Å), or 220 mm (λ = 1.7384 Å) from the crystal. X-ray images were processed using HKL2000 (61).

Structure Determination and Refinement. The crystal structure of viperin with bound SAH was determined using single-wavelength anomalous diffraction phasing based on the eight cluster Fe sites located using SHELXD (62). More than 70% of the protein residues were built automatically using the Autosol module of PHENIX (63). Automated structure refinement was performed using PHENIX (64) and accounted for translation, libration, and screw vibrational motion of partitioned chains (65) (Table S2). Manual model building was performed using Coot (66). Structural and electron density illustrations were made using Chimera (67) and PyMOL (68).

ACKNOWLEDGMENTS. Y.L. and P.C. thank Dr. Jiashee Hee for valuable discussions and Susan Mitchell for technical assistance. This work was supported by Wellcome Trust Senior Research Fellowship 101908/Z/13/Z (to Y.M.), by NIH Grants DK067081 (to S.E.E.) and GM102869 (to Y.M.), and by the Howard Hughes Medical Institute (P.C.). The work is based upon research conducted at the Advanced Photon Source on the Northeastern Collaborative Access Team beamlines, which are supported by Award GM103403 from the NIH. Use of the Advanced Photon Source is supported by the US Department of Energy, Office of Basic Energy Sciences, under Contract DE-AC02-06CH11357.

1. O'Neill LA, Bowie AG (2010) Sensing and signaling in antiviral innate immunity. *Curr Biol* 20:R328–R333.
2. Takeuchi O, Akira S (2010) Pattern recognition receptors and inflammation. *Cell* 140:805–820.
3. Isaacs A, Lindenmann J (1957) Virus interference. I. The interferon. *Proc R Soc Lond B Biol Sci* 147:258–267.
4. de Veer MJ, et al. (2001) Functional classification of interferon-stimulated genes identified using microarrays. *J Leukoc Biol* 69:912–920.
5. Der SD, Zhou A, Williams BR, Silverman RH (1998) Identification of genes differentially regulated by interferon alpha, beta, or gamma using oligonucleotide arrays. *Proc Natl Acad Sci USA* 95:15623–15628.
6. Samuel CE (2001) Antiviral actions of interferons. *Clin Microbiol Rev* 14:778–809.
7. Stark GR, Kerr IM, Williams BR, Silverman RH, Schreiber RD (1998) How cells respond to interferons. *Annu Rev Biochem* 67:227–264.
8. Chin KC, Cresswell P (2001) Viperin (cig5), an IFN-inducible antiviral protein directly induced by human cytomegalovirus. *Proc Natl Acad Sci USA* 98:15125–15130.
9. Zhu H, Cong JP, Shenk T (1997) Use of differential display analysis to assess the effect of human cytomegalovirus infection on the accumulation of cellular RNAs: Induction of interferon-responsive RNAs. *Proc Natl Acad Sci USA* 94:13985–13990.
10. Boudinot P, et al. (2000) Vesicular stomatitis virus and pseudorabies virus induce a vig1/cig5 homologue in mouse dendritic cells via different pathways. *J Gen Virol* 81:2675–2682.
11. Olofsson PS, et al. (2005) The antiviral cytomegalovirus inducible gene 5/viperin is expressed in atherosclerosis and regulated by proinflammatory agents. *Arterioscler Thromb Vasc Biol* 25:e113–e116.
12. Severa M, Coccia EM, Fitzgerald KA (2006) Toll-like receptor-dependent and -independent viperin gene expression and counter-regulation by PRDI-binding factor-1/BLIMP1. *J Biol Chem* 281:26188–26195.
13. Nasr N, et al. (2012) HIV-1 infection of human macrophages directly induces viperin which inhibits viral production. *Blood* 120:778–788.
14. Szretter KJ, et al. (2011) The interferon-inducible gene viperin restricts *West Nile virus* pathogenesis. *J Virol* 85:11557–11566.
15. Helbig KJ, et al. (2011) The antiviral protein viperin inhibits *hepatitis C virus* replication via interaction with nonstructural protein 5A. *Hepatology* 54:1506–1517.
16. Jiang D, et al. (2008) Identification of three interferon-inducible cellular enzymes that inhibit the replication of *hepatitis C virus*. *J Virol* 82:1665–1678.
17. Helbig KJ, et al. (2013) Viperin is induced following *Dengue virus* type-2 (DENV-2) infection and has anti-viral actions requiring the C-terminal end of viperin. *PLoS Negl Trop Dis* 7:e2178.
18. Wang X, Hinson ER, Cresswell P (2007) The interferon-inducible protein viperin inhibits influenza virus release by perturbing lipid rafts. *Cell Host Microbe* 2:96–105.
19. Upadhyay AS, et al. (2014) Viperin is an iron-sulfur protein that inhibits genome synthesis of tick-borne encephalitis virus via radical SAM domain activity. *Cell Microbiol* 16:834–848.
20. Fitzgerald KA (2011) The interferon inducible gene: Viperin. *J Interferon Cytokine Res* 31:131–135.
21. Sofia HJ, Chen G, Hetzler BG, Reyes-Spindola JF, Miller NE (2001) Radical SAM, a novel protein superfamily linking unresolved steps in familiar biosynthetic pathways with radical mechanisms: Functional characterization using new analysis and information visualization methods. *Nucleic Acids Res* 29:1097–1106.
22. Nicolet Y, Drennan CL (2004) AdoMet radical proteins–From structure to evolution–Alignment of divergent protein sequences reveals strong secondary structure element conservation. *Nucleic Acids Res* 32:4015–4025.
23. Berkovitch F, Nicolet Y, Wan JT, Jarrett JT, Drennan CL (2004) Crystal structure of biotin synthase, an *S*-adenosylmethionine-dependent radical enzyme. *Science* 303:76–79.
24. Broderick JB, Duffus BR, Duschene KS, Shepard EM (2014) Radical *S*-adenosylmethionine enzymes. *Chem Rev* 114:4229–4317.
25. Chatterjee A, et al. (2008) Reconstitution of ThiC in thiamine pyrimidine biosynthesis expands the radical SAM superfamily. *Nat Chem Biol* 4:758–765.
26. Fenwick MK, et al. (2015) Non-canonical active site architecture of the radical SAM thiamin pyrimidine synthase. *Nat Commun* 6:6480.
27. Frey PA, Hegeman AD, Ruzicka FJ (2008) The radical SAM superfamily. *Crit Rev Biochem Mol Biol* 43:63–88.
28. Layer G, Moser J, Heinz DW, Jahn D, Schubert WD (2003) Crystal structure of coproporphyrinogen III oxidase reveals cofactor geometry of radical SAM enzymes. *EMBO J* 22:6214–6224.
29. Lepore BW, Ruzicka FJ, Frey PA, Ringe D (2005) The x-ray crystal structure of lysine-2,3-aminomutase from *Clostridium subterminale*. *Proc Natl Acad Sci USA* 102:13819–13824.
30. Petrovich RM, Ruzicka FJ, Reed GH, Frey PA (1992) Characterization of iron-sulfur clusters in lysine 2,3-aminomutase by electron paramagnetic resonance spectroscopy. *Biochemistry* 31:10774–10781.
31. Zhang Y, et al. (2010) Diphthamide biosynthesis requires an organic radical generated by an iron-sulphur enzyme. *Nature* 465:891–896.
32. Duschene KS, Broderick JB (2010) The antiviral protein viperin is a radical SAM enzyme. *FEBS Lett* 584:1263–1267.
33. Hinson ER, Cresswell P (2009) The antiviral protein, viperin, localizes to lipid droplets via its N-terminal amphipathic alpha-helix. *Proc Natl Acad Sci USA* 106:20452–20457.
34. Hinson ER, Cresswell P (2009) The N-terminal amphipathic alpha-helix of viperin mediates localization to the cytosolic face of the endoplasmic reticulum and inhibits protein secretion. *J Biol Chem* 284:4705–4712.
35. Dosztányi Z, Csizmok V, Tompa P, Simon I (2005) IUPred: Web server for the prediction of intrinsically unstructured regions of proteins based on estimated energy content. *Bioinformatics* 21:3433–3434.
36. Walsby CJ, Ortillo D, Broderick WE, Broderick JB, Hoffman BM (2002) An anchoring role for FeS clusters: Chelation of the amino acid moiety of *S*-adenosylmethionine to the unique iron site of the [4Fe-4S] cluster of pyruvate formate-lyase activating enzyme. *J Am Chem Soc* 124:11270–11271.
37. Vey JL, Drennan CL (2011) Structural insights into radical generation by the radical SAM superfamily. *Chem Rev* 111:2487–2506.
38. Boal AK, et al. (2011) Structural basis for methyl transfer by a radical SAM enzyme. *Science* 332:1089–1092.
39. Dinis P, et al. (2015) X-ray crystallographic and EPR spectroscopic analysis of HydG, a maturase in [FeFe]-hydrogenase H-cluster assembly. *Proc Natl Acad Sci USA* 112:1362–1367.
40. Goldman PJ, Grove TL, Booker SJ, Drennan CL (2013) X-ray analysis of butirosin biosynthetic enzyme BtrN redefines structural motifs for AdoMet radical chemistry. *Proc Natl Acad Sci USA* 110:15949–15954.
41. Goldman PJ, et al. (2013) X-ray structure of an AdoMet radical activase reveals an anaerobic solution for formylglycine posttranslational modification. *Proc Natl Acad Sci USA* 110:8519–8524.
42. McLaughlin MI, et al. (2016) Crystallographic snapshots of sulfur insertion by lipoyl synthase. *Proc Natl Acad Sci USA* 113:9446–9450.
43. Nicolet Y, Amara P, Mouesca JM, Fontecilla-Camps JC (2009) Unexpected electron transfer mechanism upon AdoMet cleavage in radical SAM proteins. *Proc Natl Acad Sci USA* 106:14867–14871.
44. Chen D, Walsby C, Hoffman BM, Frey PA (2003) Coordination and mechanism of reversible cleavage of *S*-adenosylmethionine by the [4Fe-4S] center in lysine 2,3-aminomutase. *J Am Chem Soc* 125:11788–11789.
45. Kampmeier JA (2010) Regioselectivity in the homolytic cleavage of *S*-adenosylmethionine. *Biochemistry* 49:10770–10772.
46. Krissinel E, Henrick K (2007) Inference of macromolecular assemblies from crystalline state. *J Mol Biol* 372:774–797.
47. Boudinot P, Massin P, Blanco M, Riffault S, Benmansour A (1999) vig-1, a new fish gene induced by the rhabdovirus glycoprotein, has a virus-induced homologue in humans and shares conserved motifs with the MoaA family. *J Virol* 73:1846–1852.
48. Holm L, Rosenstrom P (2010) Dali server: Conservation mapping in 3D. *Nucleic Acids Res* 38:W545–W549.
49. Hänzelmann P, Schindelin H (2006) Binding of 5′-GTP to the C-terminal FeS cluster of the radical *S*-adenosylmethionine enzyme MoaA provides insights into its mechanism. *Proc Natl Acad Sci USA* 103:6829–6834.
50. Vey JL, et al. (2008) Structural basis for glycyl radical formation by pyruvate formate-lyase activating enzyme. *Proc Natl Acad Sci USA* 105:16137–16141.
51. Schwalm EL, Grove TL, Booker SJ, Boal AK (2016) Crystallographic capture of a radical *S*-adenosylmethionine enzyme in the act of modifying tRNA. *Science* 352:309–312.
52. Altschul SF, Gish W, Miller W, Myers EW, Lipman DJ (1990) Basic local alignment search tool. *J Mol Biol* 215:403–410.
53. Hover BM, Tonthat NK, Schumacher MA, Yokoyama K (2015) Mechanism of pyranopterin ring formation in molybdenum cofactor biosynthesis. *Proc Natl Acad Sci USA* 112:6347–6352.
54. Mehta AP, Abdelwahed SH, Begley TP (2015) Molybdopterin biosynthesis-mechanistic studies on a novel MoaA catalyzed insertion of a purine carbon into the ribose of GTP. *Biochim Biophys Acta* 1854:1073–1077.
55. Grove TL, et al. (2011) A radically different mechanism for *S*-adenosylmethionine-dependent methyltransferases. *Science* 332:604–607.
56. Toh SM, Xiong L, Bae T, Mankin AS (2008) The methyltransferase YfgB/RlmN is responsible for modification of adenosine 2503 in 23S rRNA. *RNA* 14:98–106.
57. Yan F, et al. (2010) RlmN and Cfr are radical SAM enzymes involved in methylation of ribosomal RNA. *J Am Chem Soc* 132:3953–3964.
58. Copley RR, Barton GJ (1994) A structural analysis of phosphate and sulphate binding sites in proteins. Estimation of propensities for binding and conservation of phosphate binding sites. *J Mol Biol* 242:321–329.
59. Mehta AP, et al. (2015) Anaerobic 5-hydroxybenzimidazole formation from aminoimidazole ribotide: An unanticipated intersection of thiamin and vitamin B12 biosynthesis. *J Am Chem Soc* 137:10444–10447.
60. Hänzelmann P, et al. (2004) Characterization of MOCS1A, an oxygen-sensitive iron-sulfur protein involved in human molybdenum cofactor biosynthesis. *J Biol Chem* 279:34721–34732.
61. Otwinoski Z, Minor W (1997) Processing of X-ray diffraction data collected in oscillation mode. *Methods Enzymol* 276:307–326.
62. Schneider TR, Sheldrick GM (2002) Substructure solution with SHELXD. *Acta Crystallogr D Biol Crystallogr* 58:1772–1779.
63. Terwilliger TC, et al. (2009) Decision-making in structure solution using Bayesian estimates of map quality: The PHENIX AutoSol wizard. *Acta Crystallogr D Biol Crystallogr* 65:582–601.
64. Adams PD, et al. (2011) The Phenix software for automated determination of macromolecular structures. *Methods* 55:94–106.
65. Painter J, Merritt EA (2006) Optimal description of a protein structure in terms of multiple groups undergoing TLS motion. *Acta Crystallogr D Biol Crystallogr* 62:439–450.
66. Emsley P, Lohkamp B, Scott WG, Cowtan K (2010) Features and development of Coot. *Acta Crystallogr D Biol Crystallogr* 66:486–501.
67. Pettersen EF, et al. (2004) UCSF Chimera–A visualization system for exploratory research and analysis. *J Comput Chem* 25:1605–1612.
68. DeLano WL (2002) *The PyMOL Molecular Graphics System* (DeLano Scientific, San Carlos, CA).
69. Dolinsky TJ, Nielsen JE, McCammon JA, Baker NA (2004) PDB2PQR: An automated pipeline for the setup of Poisson-Boltzmann electrostatics calculations. *Nucleic Acids Res* 32:W665–W667.
70. Baker NA, Sept D, Joseph S, Holst MJ, McCammon JA (2001) Electrostatics of nanosystems: Application to microtubules and the ribosome. *Proc Natl Acad Sci USA* 98:10037–10041.